

A Sparse Representation-Based Binary Hypothesis Model for Target Detection in Hyperspectral Images

Yuxiang Zhang, *Student Member, IEEE*, Bo Du, *Member, IEEE*, and Liangpei Zhang, *Senior Member, IEEE*

Abstract—In this paper, a new sparse representation-based binary hypothesis (SRBBH) model for hyperspectral target detection is proposed. The proposed approach relies on the binary hypothesis model of an unknown sample induced by sparse representation. The sample can be sparsely represented by the training samples from the background-only dictionary under the null hypothesis and the training samples from the target and background dictionary under the alternative hypothesis. The sparse vectors in the model can be recovered by a greedy algorithm, and the same sparsity levels are employed for both hypotheses. Thus, the recovery process leads to a competition between the background-only subspace and the target and background subspace, which are directly represented by the different hypotheses. The detection decision can be made by comparing the reconstruction residuals under the different hypotheses. Extensive experiments were carried out on hyperspectral images, which reveal that the SRBBH model shows an outstanding detection performance.

Index Terms—Binary hypothesis, hyperspectral imagery, sparse representation, target detection.

I. INTRODUCTION

HYPERSPECTRAL images (HSIs) have great potential for target detection because they convey abundant information about the spectral characteristics of materials, with hundreds and even thousands of bands covering specific wavelengths [1]. Target detection aims to separate the specific target pixels from the various backgrounds by the use of known target spectra or anomalous properties [2]–[5]. It has attracted significant interest in HSI applications such as detecting rare minerals in geology, oil pollution in environmental research, land mines in the public safety and defense domain, and man-made objects in reconnaissance and surveillance applications [5], [6].

Target detection algorithms are typically derived from the binary hypothesis model, which consists of two competing hypotheses: the H_0 (target absent) and H_1 (target present)

hypotheses. The test pixels in HSI can then be uniformed by implicitly or explicitly assumed statistical distribution characteristics, such as a Gaussian distribution. The likelihood ratio or generalized likelihood ratio of the probability density functions of the target and background can be conveniently used to construct a detector. Well-known algorithms with different hypothesis models include the following: 1) the spectral matched filter (SMF) [7], [8], which assumes that both hypotheses follow a Gaussian distribution and differ only in their means; 2) the matched subspace detector (MSD) [9], which assumes that both hypotheses obey a Gaussian distribution with the same scaled identity covariance matrix and differ only in their means; and 3) the adaptive coherence/cosine detectors (ACEs) [10], [11], which assume that the background has the same covariance structure but different variances under the two hypotheses.

In recent years, sparsity-based techniques have been proposed for many HSI processing fields, such as classification [12]–[14], unmixing [15], face recognition [16], [17], dimensionality reduction [18], and target detection [19]–[22]. The target detection algorithms applied with a sparsity-based approach are typically compared with the basic sparsity-based target detector (STD) proposed in [20]. The basic STD uses a similar sparsity model to that proposed in [23] to sparsely represent a test image by a few training samples, including both target and background samples, and it directly employs the reconstruction residuals to perform the detection. One of the advantages of the STD is that there is no explicit assumption on the statistical distribution characteristics of the observed data, as in the previous target detection algorithms [20]. Furthermore, compared to the algorithms with a single target spectrum, such as the SMF, the STD performs better in representing the target spectral characteristics as it uses a target subspace generated by some target training samples from a target dictionary, which can alleviate the phenomenon of spectral variability caused by the varying illumination and atmospheric effects [24], [25].

In this paper, a novel binary hypothesis model based on sparse representation (SRBBH) is proposed for HSI data. In essence, the SRBBH detector effectively combines the ideas of a binary hypothesis and sparse representation. This approach constructs more reasonable dictionaries based on the hypotheses and then sparsely and separately represents the test sample by different training samples under different hypotheses. The recovery process aims to find a certain number of atoms from the background dictionary or target and background dictionary that best represent the test pixel. Therefore, based on the same sparsity level constraint for the two hypotheses, the

Manuscript received September 10, 2013; revised December 19, 2013 and April 16, 2014; accepted June 28, 2014. This work was supported in part by the National Basic Research Program of China (973 Program) under Grants 2012CB719905 and 2011CB707105, by the National Natural Science Foundation of China under Grant 61102128, and by the Fundamental Research Funds for the Central Universities under Grant 211-274175.

Y. Zhang is with the School of Remote Sensing and Information Engineering, Wuhan University, Wuhan 430079, China (e-mail: zyx_070504@163.com).

B. Du is with the School of Computer, Wuhan University, Wuhan 430079, China (e-mail: gunspace@163.com).

L. Zhang is with the State Key Laboratory of Information Engineering in Surveying, Mapping, and Remote Sensing, Wuhan University, Wuhan 430079, China (e-mail: zlp62@whu.edu.cn).

Color versions of one or more of the figures in this paper are available online at <http://ieeexplore.ieee.org>.

Digital Object Identifier 10.1109/TGRS.2014.2337883

recovery process implicitly leads to a competition between the two hypotheses corresponding to the pixel class label. The experimental results in this paper, which are based on several different hyperspectral data sets, demonstrate that the SRBBH detector can dramatically increase the detection performance when compared to the traditional STD, and it also outperforms the other traditional detectors.

The rest of this paper is organized as follows. Section II briefly describes a number of the previously proposed approaches that are commonly used in HSI target detection. The SRBBH-driven target detection algorithm is presented in Section III. The effectiveness of the proposed model and the detection algorithm is demonstrated by extensive experiments presented in Section IV. Finally, conclusions are drawn in Section V.

II. PREVIOUS ALGORITHMS

A. MSD

In the MSD, the test pixel is modeled in terms of the target subspace and background subspace which are obtained using the target and background training samples, respectively. The competing hypotheses for the MSD are [20]

$$\begin{aligned} H_0 : \mathbf{x} &= \mathbf{B}\mathbf{b} + \mathbf{w}, \text{ target absent} \\ H_1 : \mathbf{x} &= \mathbf{S}\mathbf{t} + \mathbf{B}\mathbf{b} + \mathbf{w}, \text{ target present} \end{aligned} \quad (1)$$

where \mathbf{B} and \mathbf{S} are matrices whose columns are linearly independent and span the background and target subspaces, respectively. In the MSD, the spectral variability of the target and background are taken into account and modeled with the subspace models. \mathbf{b} and \mathbf{t} are the corresponding abundances of \mathbf{B} and \mathbf{S} . \mathbf{w} is the additive Gaussian noise, $\mathbf{w} \sim N(\mathbf{0}, \sigma_w^2 \mathbf{I})$, and σ_w^2 is the variance of the noise. Using the generalized likelihood ratio test (GLRT), the output of the MSD for an input \mathbf{x} is given by [9], [20]

$$D_{\text{MSD}}(\mathbf{x}) = \frac{\mathbf{x}^T \mathbf{P}_{\mathbf{B}}^{\perp} \mathbf{x}}{\mathbf{x}^T \mathbf{P}_{\mathbf{SB}}^{\perp} \mathbf{x}} \quad (2)$$

where $\mathbf{P}_{\mathbf{B}}^{\perp} = \mathbf{I} - \mathbf{P}_{\mathbf{B}}$ and $\mathbf{P}_{\mathbf{B}} = \mathbf{B}(\mathbf{B}^T \mathbf{B})^{-1} \mathbf{B}^T$ is the projection matrix onto the column space of the matrix \mathbf{B} . The matrix $\mathbf{SB} = [\mathbf{S} \mathbf{B}]$ denotes the matrix obtained by combining the target and background subspaces. The eigenvectors corresponding to the larger eigenvalues of the covariance matrix are usually used to generate the subspace.

B. Sparsity-Based Target Detection

A test sample \mathbf{x} is modeled to lie in the union of the background and target subspaces, respectively spanned by the background training samples $\{\mathbf{a}_i^b\}_{i=1,2,\dots,N_b}$ and the target training samples $\{\mathbf{a}_i^t\}_{i=1,2,\dots,N_t}$. Therefore, \mathbf{x} can be represented by a sparse linear combination of all the training samples [20]

$$\begin{aligned} \mathbf{x} &\approx (\alpha_1^b \mathbf{a}_1^b + \alpha_2^b \mathbf{a}_2^b + \dots + \alpha_{N_b}^b \mathbf{a}_{N_b}^b) \\ &\quad + (\alpha_1^t \mathbf{a}_1^t + \alpha_2^t \mathbf{a}_2^t + \dots + \alpha_{N_t}^t \mathbf{a}_{N_t}^t) \\ &= [\mathbf{a}_1^b \ \mathbf{a}_2^b \ \dots \ \mathbf{a}_{N_b}^b] [\alpha_1^b \ \alpha_2^b \ \dots \ \alpha_{N_b}^b]^T \\ &\quad + [\mathbf{a}_1^t \ \mathbf{a}_2^t \ \dots \ \mathbf{a}_{N_t}^t] [\alpha_1^t \ \alpha_2^t \ \dots \ \alpha_{N_t}^t]^T \\ &= \mathbf{A}^b \boldsymbol{\alpha}^b + \mathbf{A}^t \boldsymbol{\alpha}^t = \mathbf{A} \boldsymbol{\alpha} \end{aligned} \quad (3)$$

where N_b and N_t are the number of the background and target training samples, respectively. \mathbf{A}^b and \mathbf{A}^t are the $B \times N_b$ background dictionary and $B \times N_t$ target dictionary whose columns are the background and target training samples, respectively. \mathbf{A} is the union dictionary consisting of both the background and target training samples. $\boldsymbol{\alpha}$ is a concatenation of $\boldsymbol{\alpha}^b$ and $\boldsymbol{\alpha}^t$, which are sparse vectors with only a few nonzero entries.

The sparse vector $\boldsymbol{\alpha}$ can be recovered by solving

$$\hat{\boldsymbol{\alpha}} = \underset{\boldsymbol{\alpha}}{\text{argmin}} \|\mathbf{A}\boldsymbol{\alpha} - \mathbf{x}\|_2 \quad \text{subject to} \quad \|\boldsymbol{\alpha}\|_0 \leq K_0 \quad (4)$$

where $\|\cdot\|_0$ denotes the ℓ_0 -norm, which is defined as the number of nonzero entries in the vector (also called the sparsity level of the vector) [20]. K_0 is a given upper bound on the sparsity level [26]. In this paper, the aforementioned problem is solved by the orthogonal matching pursuit (OMP) [27] algorithm.

Partially reconstructed pixels, using only the background or target dictionary, can be obtained by decomposing the sparse vector $\hat{\boldsymbol{\alpha}}$ into $\hat{\boldsymbol{\alpha}}^b$ and $\hat{\boldsymbol{\alpha}}^t$, which are the vectors respectively corresponding to the background and target training samples. The recovery process implicitly leads to a competition between the background and target subspaces. The residuals of recovery by the background and target subspaces are [20]

$$\begin{aligned} r_b(\mathbf{x}) &= \|\mathbf{x} - \mathbf{A}^b \hat{\boldsymbol{\alpha}}^b\| \\ r_t(\mathbf{x}) &= \|\mathbf{x} - \mathbf{A}^t \hat{\boldsymbol{\alpha}}^t\|. \end{aligned} \quad (5)$$

The class label of the test pixel can be determined by these residuals, and the output of the detector is calculated by [20]

$$D_{\text{STD}}(\mathbf{x}) = r_b(\mathbf{x}) - r_t(\mathbf{x}). \quad (6)$$

III. SRBBH MODEL FOR TARGET DETECTION

A. SRBBH Model

Some sparse representation classifiers employ the sparsity within a class for the classification; for example, the classical sparse representation based classification [23] relies on the underlying assumption that a test sample can be linearly represented by a small number of training samples from the same class. Furthermore, the authors in [20] showed that a few background samples are adequate to reconstruct a test background sample in HSI. Thus, for a background pixel \mathbf{x} , its spectrum can be approximately represented as a linear combination of the training samples $\{\mathbf{a}_i^b\}_{i=1,2,\dots,N_b}$ as follows:

$$\begin{aligned} \mathbf{x} &\approx \gamma_1 \mathbf{a}_1^b + \gamma_2 \mathbf{a}_2^b + \dots + \gamma_{N_b} \mathbf{a}_{N_b}^b \\ &= [\mathbf{a}_1^b \ \mathbf{a}_2^b \ \dots \ \mathbf{a}_{N_b}^b] [\gamma_1 \ \gamma_2 \ \dots \ \gamma_{N_b}]^T \\ &= \mathbf{A}^b \boldsymbol{\gamma} \end{aligned} \quad (7)$$

where $\boldsymbol{\gamma}$ is a sparse vector whose entries are the abundances of the corresponding training samples in the background dictionary \mathbf{A}^b .

Similarly, if \mathbf{x} is a target pixel, particularly a subpixel target, its spectrum approximately lies in a low-dimensional subspace spanned by the union of the background training samples $\{\mathbf{a}_i^b\}_{i=1,2,\dots,N_b}$ and the target training samples $\{\mathbf{a}_i^t\}_{i=1,2,\dots,N_t}$.

The pixel \mathbf{x} can be approximately represented as a linear combination of all the training samples as follows:

$$\begin{aligned} \mathbf{x} &\approx (\beta_1^b \mathbf{a}_1^b + \beta_2^b \mathbf{a}_2^b + \cdots + \beta_{N_b}^b \mathbf{a}_{N_b}^b) \\ &\quad + (\beta_1^t \mathbf{a}_1^t + \beta_2^t \mathbf{a}_2^t + \cdots + \beta_{N_t}^t \mathbf{a}_{N_t}^t) \\ &= [\mathbf{a}_1^b \ \mathbf{a}_2^b \ \cdots \ \mathbf{a}_{N_b}^b][\beta_1^b \ \beta_2^b \ \cdots \ \beta_{N_b}^b]^T \\ &\quad + [\mathbf{a}_1^t \ \mathbf{a}_2^t \ \cdots \ \mathbf{a}_{N_t}^t][\beta_1^t \ \beta_2^t \ \cdots \ \beta_{N_t}^t]^T \\ &= \mathbf{A}^b \boldsymbol{\beta}^b + \mathbf{A}^t \boldsymbol{\beta}^t = \mathbf{A} \boldsymbol{\beta} \end{aligned} \quad (8)$$

where $\mathbf{A} = [\mathbf{A}^b \ \mathbf{A}^t]$ is the $B \times (N_b + N_t)$ union dictionary consisting of both the background dictionary \mathbf{A}^b and the target dictionary \mathbf{A}^t . $\boldsymbol{\beta}^b$ and $\boldsymbol{\beta}^t$ are the unknown vectors whose entries are the abundances of the corresponding background and target training samples, respectively. $\boldsymbol{\beta}$ is a concatenation of $\boldsymbol{\beta}^b$ and $\boldsymbol{\beta}^t$ and is a sparse vector.

In the proposed detection algorithm, an unknown test sample is modeled to lie in the background subspace or the target and background subspace. Therefore, a test sample \mathbf{x} can be chosen from the competing hypotheses

$$\begin{aligned} H_0 : \mathbf{x} &= \mathbf{A}^b \boldsymbol{\gamma} + \mathbf{e}_0, \quad \text{target absent} \\ H_1 : \mathbf{x} &= \mathbf{A}^b \boldsymbol{\beta}^b + \mathbf{A}^t \boldsymbol{\beta}^t + \mathbf{e}_1 = \mathbf{A} \boldsymbol{\beta} + \mathbf{e}_1, \quad \text{target present} \end{aligned} \quad (9)$$

where \mathbf{e}_0 and \mathbf{e}_1 are the approximation residuals, and the same sparsity constraint is employed for both hypotheses, which makes the two residuals more comparable. The constraint is further discussed in the following part and clearly examined in the experiment section.

This model is similar to the MSD [9]. However, in the case of the MSD, the target and background are assumed to have a Gaussian distribution, the unknown parameters can be estimated by the maximum likelihood estimation method, and GLRT is used to develop the detector. In the proposed SRBBH model, no assumption about the target and background distributions is required, and a greedy algorithm is used to estimate the unknown sparse vectors. The approximate residuals can then be easily obtained by a subtract operation and are directly used to develop the detector.

In addition, in the MSD signal model, the columns of the background and target dictionaries have to be independent in order to generate the required projection operators, and the eigenvectors corresponding to the significant eigenvalues of the target and background covariance matrices are usually used to generate the columns of the background and target dictionaries. In the proposed approach, the subspace model is more generalized since independence between the training samples is not necessary.

The proposed SRBBH model is more complete and realistic than the basic sparsity model in STD [20]. The basic sparsity model in STD can be regarded as a special case of the SRBBH model. In the case of the basic sparsity model, either the target test samples or the background test samples are represented by both the background and target training samples. In the proposed SRBBH model, the test samples are modeled separately with more reasonable dictionaries, only the background training samples for the null hypothesis, and the combined target and background training samples for the alternative hypothesis.

The basic sparsity model in STD does not fully incorporate the class label (prior) information of the data set; it only utilizes the class label (background and target) information in postprocessing when calculating the residuals for each class and ignores it when calculating the sparse vectors. In the detection problems, we are given a set of training samples with corresponding labels, although the available number of training samples will be very limited, particularly the target training samples. The proposed SRBBH model makes the assumption that a test sample should be represented by the atoms from the same classes that the test sample belongs to, which means that the test sample is modeled separately, with the training samples from different classes for the different hypotheses.

Furthermore, in the basic sparsity model in STD, the recovery process implicitly leads to a competition between the background and target subspaces, respectively spanned by the background and target training samples. In the proposed SRBBH model, the recovery process implicitly leads to a competition between the null hypothesis represented by the background subspace and the alternative hypothesis represented by the background and target subspace.

Moreover, as for the computational complexity, since SRBBH-based target detector (SRBBH-TD) solves two STD-like optimization problems, the time cost of SRBBH-TD is about twice as that of STD.

B. Reconstruction and Detection

Given the dictionaries \mathbf{A}^b and \mathbf{A} , the sparse vectors $\boldsymbol{\gamma}$ and $\boldsymbol{\beta}$ can be obtained by solving the problem in (4), which, in this paper, is achieved with the OMP [27] algorithm.

The sparse vectors $\hat{\boldsymbol{\gamma}}$ and $\hat{\boldsymbol{\beta}}$ are therefore recovered to find the few atoms that best represent the test pixel under the different hypotheses. In addition, the test sample can be reconstructed by $\hat{\mathbf{x}}_0 = \mathbf{A}^b \hat{\boldsymbol{\gamma}}$ and $\hat{\mathbf{x}}_1 = \mathbf{A} \hat{\boldsymbol{\beta}}$, where $\hat{\boldsymbol{\gamma}}$ and $\hat{\boldsymbol{\beta}}$ are the recovered sparse vectors corresponding to \mathbf{A}^b and \mathbf{A} . The recovery process implicitly leads to a competition between the two hypotheses. The recovered sparse representation is therefore naturally discriminative. The reconstructed spectrum can be determined by comparing the reconstruction error of the mean squared error under the two hypotheses. The residuals of recovery by the two hypotheses are

$$\begin{aligned} r_0(\mathbf{x}) &= \|\mathbf{x} - \mathbf{A}^b \hat{\boldsymbol{\gamma}}\| \\ r_1(\mathbf{x}) &= \|\mathbf{x} - \mathbf{A} \hat{\boldsymbol{\beta}}\|. \end{aligned} \quad (10)$$

The class label of the test pixel can be determined by these residuals. In addition, the output of the SRBBH-TD is calculated by

$$D_{\text{SRBBH-TD}}(\mathbf{x}) = r_0(\mathbf{x}) - r_1(\mathbf{x}). \quad (11)$$

OMP is a greedy algorithm which terminates when the following occurs: 1) A prescribed sparsity level is reached, or 2) the residual becomes sufficiently small. In our proposed problem setting, the second stopping criterion should be removed because the detection is completely based on the approximate residual. The sparsity level which controls the

approximation accuracy therefore becomes a critical parameter. The sparsity level refers to the number of nonzero entries in the sparse vector, which is also the number of atoms selected from the dictionary by OMP to approximate the test pixel.

Whether the same values of the sparsity level parameters should be used in both hypotheses during the recovery process is an interesting problem. If the values are set differently in both hypotheses, and especially if the value of the sparsity level parameter in H_1 is higher than that in the null hypothesis, from a reconstruction point of view, the target and background subspace will therefore have a higher dimension with a richer basis and, consequently, it is likely to represent the test pixel (background or target) more accurately. Thus, it is highly likely that the H_1 residual should be smaller than the H_0 residual, and it may lead to a significantly biased misclassification and a weakened competition between both hypotheses. Contrary, if the value of the sparsity level parameter in H_1 is smaller than that in the null hypothesis, for a background test pixel, the H_0 residual is highly likely to be smaller than the H_1 residual, and it is likely to lead to a correct classification; for a target test pixel, the relationship between two residuals in H_0 and H_1 may be not certain. In brief, different values of the sparsity level parameters are likely to lead to a significantly weakened competition between both hypotheses and a severely biased misclassification; hence, the same values of the sparsity level parameters should be used in both hypotheses, which can also greatly help to reduce the complexity of the parameter adjustment. As we know, the recovery process aims to find a certain number of atoms from \mathbf{A}^b or \mathbf{A} that best represent the test pixel. Therefore, when the same values of the sparsity level parameters are set for both hypotheses, for a background test pixel, the reconstruction residuals of the two hypotheses tend to be the same. For a target pixel, the reconstruction residual via target and background samples in \mathbf{A} tends to be smaller than that through the same number of only background samples in \mathbf{A}^b . Therefore, based on the same sparsity level constraint, the recovery process implicitly leads to a better competition between the two hypotheses, which will be further examined in the experiment section.

C. Background and Union Dictionary Construction

The construction of dictionaries \mathbf{A}^b and \mathbf{A} requires careful attention. A universal dictionary constructed via the training samples in the whole image scene can guarantee the sparsity in the coefficient vector. However, in return, it makes the solution of the coefficient vector unstable, and there will be a lot of atoms which are uncorrelated to the test sample. Furthermore, in target detection applications, there is usually a large time consumption for recovering the sparse vector by a large universal dictionary. In this paper, an adaptive local dictionary method [20] is employed to construct the background dictionary in order to better represent and capture the spectral signature of the test sample. The number of the target pixels is small. The target dictionary is therefore constructed from some of the target pixels in the global image scene. Specifically, the background dictionary is generated locally for each test pixel through a dual concentric window which separates the local area around each

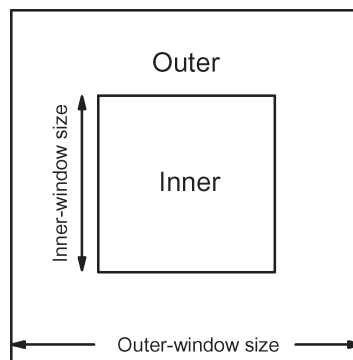


Fig. 1. Dual concentric window and its window sizes.

pixel into two regions, a small inner window region (IWR) centered within a larger outer window region (OWR) [28], as shown in Fig. 1. The IWR is used to enclose the target of interest to be detected, while the OWR is employed to model the local background around the target region. Since there is no specific method to choose the size of the detection window [29], the window sizes are set manually and experientially. Only pixels in the outer region form the atoms in \mathbf{A}^b . In this way, the subspace spanned by the background dictionary becomes adaptive to the local statistics. Therefore, if the test sample is a background pixel, it is likely to find very similar spectral characteristics in the background dictionary. On the other hand, if the test sample is a target pixel, particularly a target embedded as a single pixel, it will be difficult for the pixel to find a good match in \mathbf{A}^b since the OWR does not include any target pixels, and the test pixel is likely to be better represented by the target and background dictionary \mathbf{A} under the H_1 hypothesis.

As with the local detectors, the center window in the dual-window structure is a guard window which is used to eliminate the probable targets in the outer window so that the background dictionary is pure. However, targets in the outer window may still exist and make the outer window impure since the windows slide across the whole image. This is a common problem for all the local detectors. We can expect that if the target pixels are distributed densely and evenly, the problem may have a great effect on the detection performance; otherwise, it tends to be ignored. One way to solve the problem is to exclude the probable target pixels by the prior target spectrum before dictionary construction. We can undertake this target exclusion procedure and then construct the background dictionary from the outer window.

According to the aforementioned descriptions, the SRBBH model for hyperspectral target detection is presented in Table I.

IV. HYPERSPECTRAL DATA EXPERIMENTS

A. Hyperspectral Data Sets

Three hyperspectral data sets are used in this paper to evaluate the effectiveness of the proposed detectors introduced in Section III. We use three data sets with different characteristics, including the data collection instrument, the target size, and the spatial distribution of the targets.

TABLE I
PROPOSED SRBBHD-TD ALGORITHM FOR HSI

1. **Input:** a hyperspectral image and parameters: 1) the two sizes of dual window; 2) the sparsity level of OMP;
2. **Preprocessing:**
Choose the target atoms $\{\mathbf{a}_i^t\}_{i=1,2,\dots,N_t}$;
3. **For** each test pixel \mathbf{x} in the image scene:
 - 1) Construct a background dictionary falling into the OWR;
 - 2) Construct a union background and target dictionary;
 - 3) Compute the detection statistics via (11)
 - 4) Turn to the next pixel**End for**
4. **Output:** maps of the detection statistics of each pixel.

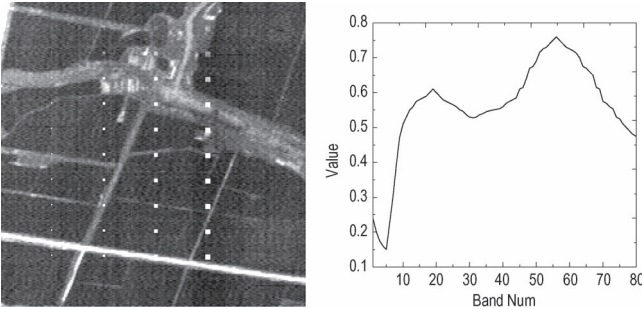


Fig. 2. PHI image scene of band 10 and the signature of the target material.

The first data set is a synthetic image, which was collected by the Chinese-made push-broom hyperspectral imager (PHI). It is a scene of the Xia Qiao Field in Liyang City, Changzhou City, Jiangsu Province, China. The image scene covers an area of 240×240 pixels, with 80 spectral bands in wavelengths ranging from 400 to 850 nm. The spectral resolution is 5 nm.

To evaluate the performance of the proposed algorithm with a wide variety of subpixel targets, a target implant method [30] is used in this paper. Based on a linear mixing model, a synthetic subpixel target with spectrum \mathbf{z} is generated by fractionally implanting a desired target with spectrum \mathbf{t} in a given pixel of the background with spectrum \mathbf{b} as follows [31]:

$$\mathbf{z} = f \cdot \mathbf{t} + (1 - f) \cdot \mathbf{b}. \quad (12)$$

In order to generate the targets, 40 panels are implanted in a spatial grid, distributed in ten rows and four columns. The sizes of the panels in the first, second, third, and fourth columns are (in pixels) as follows: 1×1 , 2×2 , 3×3 , and 4×4 , respectively. There are four panels and 30 target pixels in each row and 300 target pixels in the whole image scene. The andradite is selected as the target material from the Environment for Visualizing Images (ENVI) standard spectral library, and the target spectrum is shown in Fig. 2. Each row of the panels is made up of subpixels with 5%, 10%, 15%, 20%, 25%, 30%, 35%, 40%, 45%, or 50% abundance of the target material, and the rest is background. An image of band 10 from this data set is shown in Fig. 2.

The second data set was collected by the Hyperspectral Digital Image Collection Experiment (HYDICE) sensor. The data set has 210 spectral bands in the visible–near-infrared range. The spatial resolution is 2 m, and the spectral resolution is 10 nm. After removing the water absorption, low SNR, and

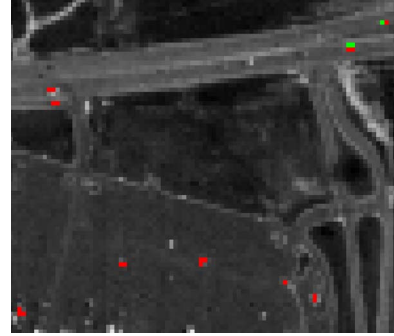


Fig. 3. HYDICE image scene.



Fig. 4. AVIRIS image scene and the target locations.

bad bands (1–4, 76, 87, 101–111, 136–153, and 198–210), 162 bands of the data are retained. The image scene is 150×150 pixels, as shown in Fig. 3. This data set is an urban scene in which there are nine vehicles, including 21 target pixels as targets to be detected.

The third data set was collected by the Airborne Visible/Infrared Imaging Spectrometer (AVIRIS) from San Diego, CA, USA. The spatial resolution is 3.5 m per pixel. The image has 224 spectral channels in wavelengths ranging from 370 to 2510 nm. After removing the bands that correspond to the water absorption regions, low SNR, and bad bands (1–6, 33–35, 97, 107–113, 153–166, and 221–224), 189 available bands of the data are retained in the experiments. From this hyperspectral data set, a region with the size of 200×240 pixels is selected to test the detection performance, as shown in Fig. 4. There are six planes including 90 target pixels as targets to be detected in the scene, as shown in Fig. 4.

B. Experiment Settings

For the PHI data set, the spectral signatures of the target training samples $\{\mathbf{a}_i^t\}_{i=1,2,\dots,N_t}$ are collected from $N_t = 16$ pixels from a 4×4 panel of the tenth row. The background signatures $\{\mathbf{a}_i^b\}_{i=1,2,\dots,N_b}$ are generated by the pixels in the outer region of a dual window. The sizes of the OWR and IWR are set as 17×17 and 7×7 , respectively, and there are $N_b = 240$ background training samples.

For the HYDICE data set, the spectral signatures of the target $\{\mathbf{a}_i^t\}_{i=1,2,\dots,N_t}$ are collected from $N_t = 3$ pixels from the two targets marked in green, as shown in Fig. 3. The sizes of the OWR and IWR are set as 19×19 and 5×5 , respectively, and there are $N_b = 336$ background training samples $\{\mathbf{a}_i^b\}_{i=1,2,\dots,N_b}$.

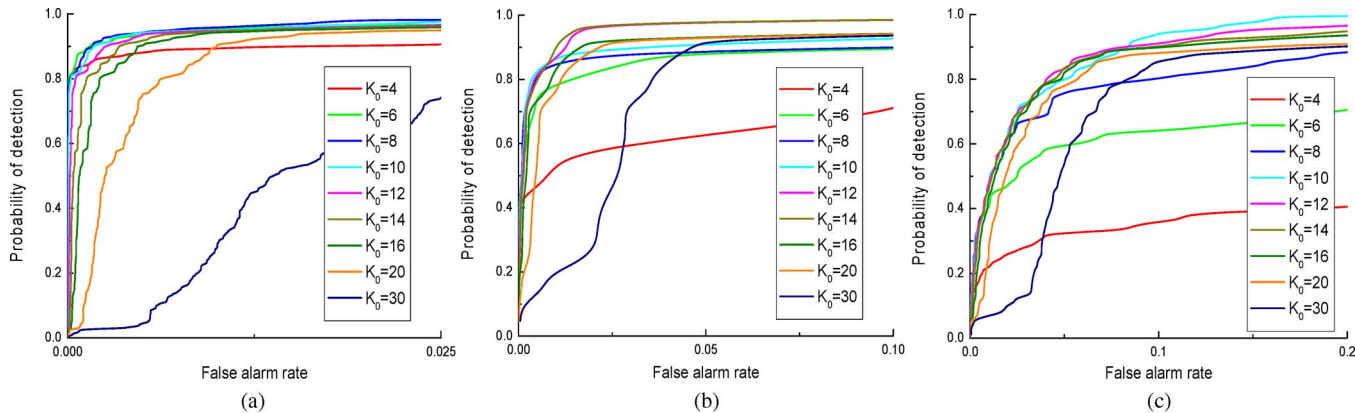


Fig. 5. Effect of the sparsity level on the detection performance of SRBBH-TD. (a) PHI. (b) HYDICE. (c) AVIRIS.

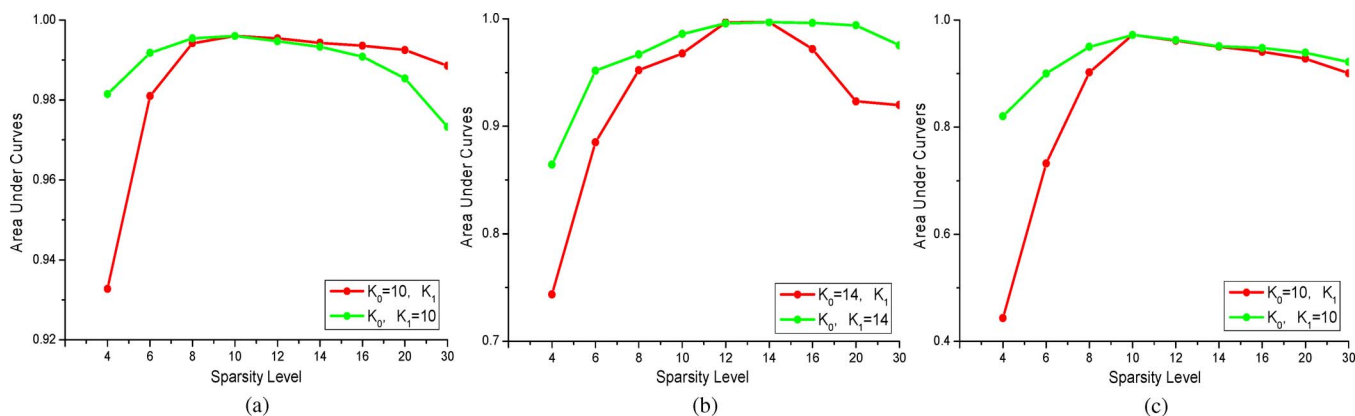


Fig. 6. AUC comparison for three data sets at different sparsity levels for both hypotheses in SRBBH-TD. (a) PHI. (b) HYDICE. (c) AVIRIS.

For the AVIRIS data set, we select one pixel from each plane as the target atoms, and $N_t = 6$. The sizes of the OWR and IWR are set as 17×17 and 7×7 , respectively, and $N_b = 240$.

SRBBH-TD is compared to the following algorithms: 1) SMF; 2) MSD; 3) ACE; and 4) STD. For all the detectors, we use the same given target spectrum as the input *a priori* target spectrum. In the case of SMF, the target signature is the mean of the target atoms $\{\mathbf{a}_i^t\}_{i=1,2,\dots,N_t}$. We adopt the pixels falling in the OWR to estimate the background covariance matrix in the SMF and ACE algorithms and to construct the background atoms in STD and SRBBH-TD. In the case of MSD, the eigenvectors corresponding to the significant eigenvalues of the covariance matrices obtained from the training atoms are used to generate the basis for the subspaces [32].

C. Detection Performance

First, we demonstrate how the detection results of SRBBH-TD are affected by the sparsity level of the representation. The receiver operating characteristic (ROC) curves for the three images, using the OMP with sparsity levels $K_0 = 4, 6, 8, 10, 12, 14, 16, 20,$ and 30 , are shown in Fig. 5(a)–(c). For a very small K_0 , the sparsity-based techniques are reduced to a simple template matching and lead to underfitting, which leads to a weakening of the final target detection performance. For example, when $K_0 = 4$, there is an inferior detection performance for all three data sets, particularly the

AVIRIS data set. In general, the detection performance improves as the sparsity level K_0 increases to a certain level. However, if K_0 is too large, the solution becomes dense and involves both the background and target atoms, particularly in the null hypothesis, and thus, its discriminative power is reduced. In this paper, the sparsity level K_0 is chosen to be close to the size of the target dictionary. When comparing the detection performance with different values of K_0 , the optimal value of K_0 for the proposed SRBBH-TD algorithm in the PHI, HYDICE, and AVIRIS data sets is 10, 14, and 10, respectively. In a similar way, the optimal value of K_0 for the STD algorithm in the three data sets is 6, 4, and 4, respectively.

Second, the effectiveness of the same sparsity level constraint is examined by comparing the detection performance when the sparsity levels for two hypotheses (K_0 for H_0 and K_1 for H_1) are different. From the aforementioned experiment results, when the sparsity levels are set as the same in SRBBH-TD, the optimal value for the PHI, HYDICE, and AVIRIS data sets is 10, 14, and 10, respectively. Therefore, in the following experiment, we will group the experiment into two parts for each data set, examining the detection performance of SRBBH-TD when $K_0 = 4, 6, 8, 10, 12, 14, 16, 20,$ and 30 and K_1 is fixed as the optimal value and then examining the detection performance of SRBBH-TD when K_0 is fixed as the optimal value and $K_1 = 4, 6, 8, 10, 12, 14, 16, 20,$ and 30 . The area under the curve (AUC) curves are shown in Fig. 6. We can

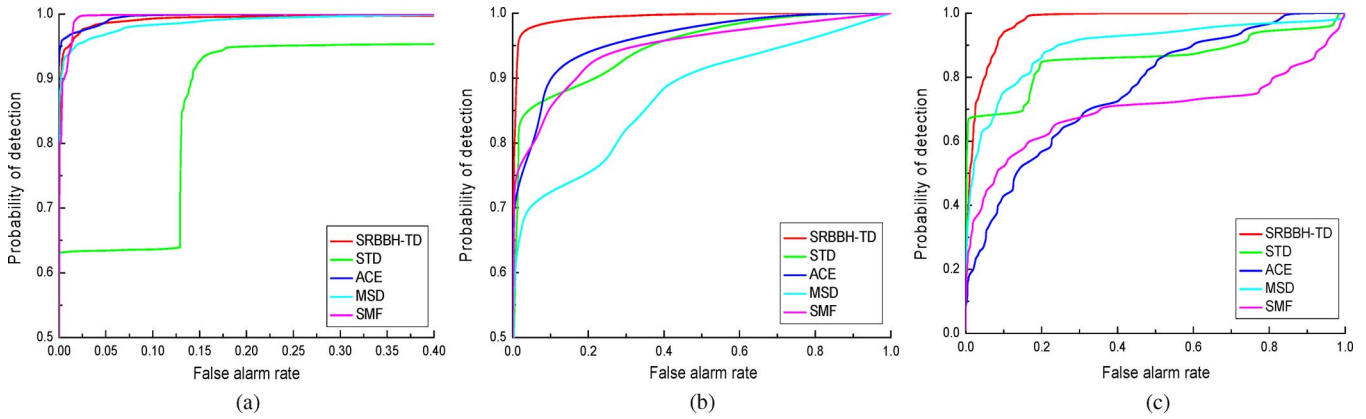


Fig. 7. Detection performance comparison of five detectors for the three data sets. (a) PHI. (b) HYDICE. (c) AVIRIS.

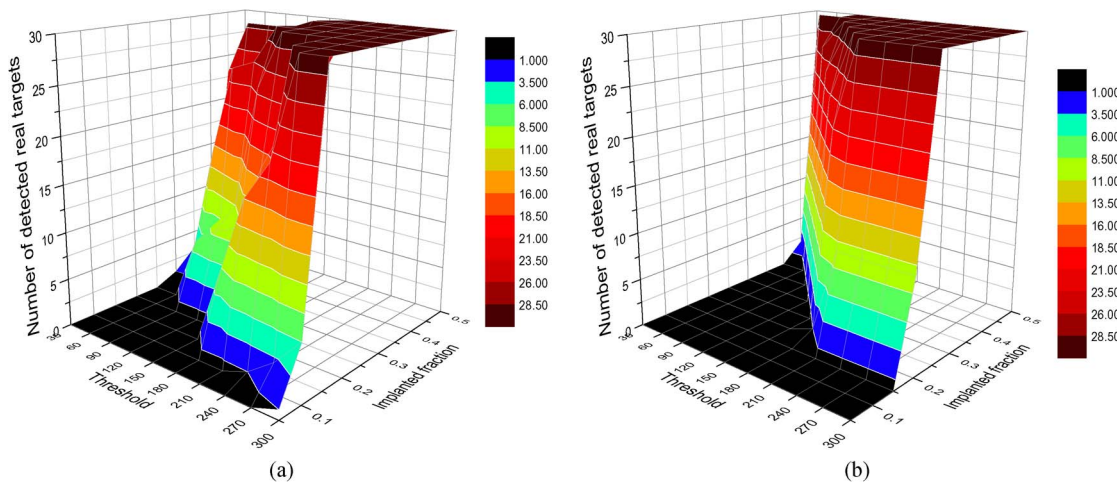


Fig. 8. Detection performance for targets with different implanted fractions by two methods. (a) SRBBH-TD. (b) STD.

clearly see that the two curves will cross each other above the so-called optimal value of sparsity level. Moreover, the crossing point is the peak of the AUC curves, which means that SRBBH-TD will obtain better detection performance when the sparsity levels are set as the same for both hypotheses.

Third, the detection performance of the proposed detector is evaluated. The sparsity level is set as the aforementioned optimal value in the three data sets. The experimental results for the five detectors are provided through ROC curves, as shown in Fig. 7. This shows that the proposed SRBBH-TD performs significantly better than STD in all three data sets, and SRBBH-TD outperforms all the other detectors in the HYDICE and AVIRIS data sets. STD, in particular, performs poorly in the PHI data set, which may be related to the implanted fraction of the targets in the image scene.

The performance in detecting subpixel targets with different fractions is now further analyzed. The sparsity level is again set as the aforementioned optimal value. The experimental results presented by a 3-D surface are shown in Fig. 8. The X, Y, and Z axes respectively represent the threshold, the implanted target fraction, and the number of the detected real targets. The number of the real targets at each fraction is 30. When the detection value $D(x)$ of the input pixel is larger than a particular value y , then the input test pixel will be declared as a target. If the real implanted targets present detection values

larger than y , then they can be labeled as detected real targets. For simplicity and consistency, the detection values of all the pixels in the image scene are sorted according to descending order, and the threshold η is set to segment a certain number of pixels with the largest detection values, such as 30, 60, 90, 120, 150, 180, 210, 240, 270, and 300. The number of detected real target pixels can be computed from these different segmented results by inspecting the target references.

The results clearly show that the dark region of the surface by STD is larger than that by SRBBH-TD. The dark area indicates that the number of detected real targets is zero at an implanted target fraction and threshold. Therefore, the results demonstrate that SRBBH-TD outperforms STD in detecting subpixel targets. In detail, when the threshold is 30, SRBBH-TD can detect one target pixel with a 30% target fraction, three target pixels with a 35% target fraction, and one target pixel with a 40% target fraction, but STD cannot detect target pixels with a fraction of less than 40%. When the threshold reaches 300, SRBBH-TD can detect one target pixel with a 5% target fraction, six target pixels with a 10% target fraction, and all the target pixels with a target fraction of more than 10%. Meanwhile, STD can detect ten target pixels with a 20% target fraction and all the target pixels with a target fraction of more than 20%. With the other thresholds, it is a similar case.

V. CONCLUSION

This paper proposes a SRBBH model for target detection in hyperspectral imagery. In the proposed model, the pixel observation can be effectively and separately represented by different sparse representations under different hypotheses: The pixel spectrum can be modeled by the background training samples under the null hypothesis and by both the target and background training samples under the alternative hypothesis. In this way, the pixel can be modeled by different representations according to its label (target or background), incorporating the prior information of the class label for the training samples. In the proposed detector, the sparse representation is recovered by the OMP algorithm, and the sparsity level in both hypotheses is set as the same. The detection decision can be obtained from the reconstruction residuals.

The proposed algorithm and several state-of-the-art detectors were implemented with different sparsity levels in three HSIs. The experiment results reveal the following: 1) The proposed model with reasonable dictionaries outperforms the original STD model in separating the target from background; 2) the same sparsity level constraint is suitable for SRBBH model, which will make the SRBBH-TD obtain a better detection performance; 3) the value of the sparsity level is roughly around the size of the target dictionary, and it is therefore easy to determine the value of the sparsity level; and 4) in general, the proposed SRBBH model is effective for hyperspectral target detection, particularly for subpixel target detection.

Our future research will investigate the construction of better dictionaries, such as a pure background dictionary. The target dictionary is randomly collected from the training data, and the performance of the proposed detector can vary with the dictionary. We will therefore focus on how to automatically construct an optimal target dictionary. We will also investigate the computational complexity of the detector.

ACKNOWLEDGMENT

The authors would like to thank the handling editor and anonymous reviewers for their careful reading and helpful remarks.

REFERENCES

- [1] M. Borengasser, W. S. Hungate, and R. Watkins, *Hyperspectral Remote Sensing—Principles and Applications*. Boca Raton, FL, USA: CRC Press, 2008.
- [2] D. Manolakis, C. Siracusa, and G. Shaw, "Hyperspectral subpixel target detection using the linear mixing model," *IEEE Trans. Geosci. Remote Sens.*, vol. 39, no. 7, pp. 1392–1409, Jul. 2001.
- [3] J. P. Kerekes and J. E. Baum, "Spectral imaging system analytical model for subpixel object detection," *IEEE Trans. Geosci. Remote Sens.*, vol. 40, no. 5, pp. 1088–1101, May 2002.
- [4] M. S. Stefanou and J. P. Kerekes, "Image-derived prediction of spectral image utility for target detection applications," *IEEE Trans. Geosci. Remote Sens.*, vol. 48, no. 4, pp. 1827–1833, Apr. 2010.
- [5] D. Manolakis and G. Shaw, "Detection algorithms for hyperspectral imaging applications," *IEEE Signal Process. Mag.*, vol. 19, no. 1, pp. 29–43, Jan. 2002.
- [6] S. Matteoli, M. Diani, and G. Corsini, "A tutorial overview of anomaly detection in hyperspectral images," *IEEE Aerosp. Electron. Syst. Mag.*, vol. 25, no. 7, pp. 5–28, Jul. 2010.
- [7] D. Manolakis, G. Shaw, and N. Keshava, "Comparative analysis of hyperspectral adaptive matched filter detectors," in *Proc. SPIE Conf. Algorithms Multispectr., Hyperspectr., Ultraspectr. Imagery 6*, Apr. 2000, vol. 4049, pp. 2–17.
- [8] N. M. Nasrabadi, "Regularized spectral matched filter for target recognition in hyperspectral imagery," *IEEE Signal Process. Lett.*, vol. 15, pp. 317–320, 2008.
- [9] L. L. Scharf and B. Friedlander, "Matched subspace detectors," *IEEE Trans. Signal Process.*, vol. 42, no. 8, pp. 2146–2157, Aug. 1994.
- [10] D. Manolakis, D. Marden, and G. A. Shaw, "Hyperspectral image processing for automatic target detection applications," *J. Lincoln Lab.*, vol. 14, no. 1, pp. 79–116, 2003.
- [11] S. Kraut, L. L. Scharf, and L. T. McWhorter, "Adaptive subspace detectors," *IEEE Trans. Signal Process.*, vol. 49, no. 1, pp. 1–16, Jan. 2001.
- [12] X. Hang and F.-X. Wu, "Sparse representation for classification of tumors using gene expression data," *J. Biomed. Biotechnol.*, vol. 2009, pp. 1–6, 2009.
- [13] Y. Chen, N. M. Nasrabadi, and T. D. Tran, "Hyperspectral image classification via kernel sparse representation," *IEEE Trans. Geosci. Remote Sens.*, vol. 51, no. 1, pp. 217–231, Jan. 2013.
- [14] U. Srinivas, Y. Chen, V. Monga, N. M. Nasrabadi, and T. D. Tran, "Exploiting sparsity in hyperspectral image classification via graphical models," *IEEE Geosci. Remote Sens. Lett.*, vol. 10, no. 3, pp. 505–509, May 2013.
- [15] Z. Guo, T. Wittman, and S. Osher, "L1 unmixing and its application to hyperspectral image enhancement," in *Proc. SPIE Conf. Algorithms Technol. Multispectr., Hyperspectr., Ultraspectr. Imagery 15*, Apr. 2009, vol. 7334, pp. 1–9.
- [16] L. Zhang, M. Yang, and X. Feng, "Sparse representation or collaborative representation: Which helps face recognition?" in *Proc. IEEE Int. Conf. Comput. Vis.*, 2011, pp. 471–478.
- [17] Y. Yuan, X. Li, Y. Pang, X. Lu, and D. Tao, "Binary sparse nonnegative matrix factorization," *IEEE Trans. Circuits Syst. Video Technol.*, vol. 19, no. 5, pp. 772–777, May 2009.
- [18] Y. Han, F. Wu, D. Tao, and J. shao, "Sparse unsupervised dimensionality reduction for multiple view data," *IEEE Trans. Circuits Syst. Video Technol.*, vol. 22, no. 10, pp. 1485–1496, Oct. 2012.
- [19] L. Zhang, L. Zhang, D. Tao, and X. Huang, "Sparse transfer manifold embedding for hyperspectral target detection," *IEEE Trans. Geosci. Remote Sens.*, vol. 52, no. 2, pp. 1030–1043, Mar. 2014.
- [20] Y. Chen, N. M. Nasrabadi, and T. D. Tran, "Sparse representation for target detection in hyperspectral imagery," *IEEE J. Sel. Topics Signal Process.*, vol. 5, no. 3, pp. 629–640, Jun. 2011.
- [21] Y. Chen, N. M. Nasrabadi, and T. D. Tran, "Simultaneous joint sparsity model for target detection in hyperspectral imagery," *IEEE Geosci. Remote Sens. Lett.*, vol. 8, no. 4, pp. 676–680, Jul. 2011.
- [22] Y. Chen, N. M. Nasrabadi, and T. D. Tran, "Kernel sparse representation for hyperspectral target detection," in *Proc. IEEE IGARSS*, 2012, pp. 7484–7487.
- [23] J. Wright, A. Y. Yang, A. Ganesh, S. Sastry, and Y. Ma, "Robust face recognition via sparse representation," *IEEE Trans. Pattern Anal. Mach. Intell.*, vol. 31, no. 2, pp. 210–227, Feb. 2009.
- [24] G. Healey and D. Slater, "Models and methods for automated material identification in hyperspectral imagery acquired under unknown illumination and atmospheric conditions," *IEEE Trans. Geosci. Remote Sens.*, vol. 37, no. 6, pp. 2706–2717, Jun. 1999.
- [25] B. Thai and G. Healey, "Invariant subpixel material detection in hyperspectral imagery," *IEEE Trans. Geosci. Remote Sens.*, vol. 40, no. 3, pp. 599–608, Mar. 2002.
- [26] J. A. Tropp and S. J. Wright, "Computational methods for sparse solution of linear inverse problems," *Proc. IEEE*, vol. 98, no. 6, pp. 948–958, Jun. 2010.
- [27] J. A. Tropp and A. C. Gilbert, "Signal recovery from random measurements via orthogonal matching pursuit," *IEEE Trans. Inf. Theory*, vol. 53, no. 12, pp. 4655–4666, Dec. 2007.
- [28] H. Kwon, S. Z. Der, and N. M. Nasrabadi, "Dual-window-based anomaly detection for hyperspectral imagery," in *Proc. SPIE*, 2003, vol. 5094, pp. 148–158.
- [29] A. Banerjee, P. Burlina, and C. Diehl, "A support vector method for anomaly detection in hyperspectral imagery," *IEEE Trans. Geosci. Remote Sens.*, vol. 44, no. 8, pp. 2282–2291, Aug. 2006.
- [30] M. S. Stefanou and J. P. Kerekes, "A method for assessing spectral image utility," *IEEE Trans. Geosci. Remote Sens.*, vol. 47, no. 6, pp. 1698–1706, Jun. 2009.
- [31] S. M. Schweizer and J. M. F. Moura, "Efficient detection in hyperspectral imagery," *IEEE Trans. Image Process.*, vol. 10, no. 4, pp. 584–597, Apr. 2001.
- [32] H. Kwon and N. M. Nasrabadi, "A comparative analysis of kernel subspace target detectors for hyperspectral imagery," *EURASIP J. Appl. Signal Process.*, vol. 2007, no. 1, pp. 193–193, Jan. 2007.



Yuxiang Zhang (S'13) received the B.S. degree in sciences and techniques of remote sensing from Wuhan University, Wuhan, China, in 2011, where she is currently working toward the Ph.D. degree in sciences and techniques of remote sensing.

Her research interests include hyperspectral image processing, target detection, sparse representation, and signal processing.



Liangpei Zhang (M'06–SM'08) received the B.S. degree in physics from Hunan Normal University, Changsha, China, in 1982, the M.S. degree in optics from the Xi'an Institute of Optics and Precision Mechanics, Chinese Academy of Sciences, Xi'an, China, in 1988, and the Ph.D. degree in photogrammetry and remote sensing from Wuhan University, Wuhan, China, in 1998.

He is currently the Head of the Remote Sensing Division, State Key Laboratory of Information Engineering in Surveying, Mapping, and Remote Sensing, Wuhan University. He is also a "Chang-Jiang Scholar" Chair Professor appointed by the Ministry of Education of China. He is currently a Principal Scientist for the China State Key Basic Research Project (2011–2016) appointed by the Ministry of National Science and Technology of China to lead the remote sensing program in China. He has more than 300 research papers. He is the holder of five patents. His research interests include hyperspectral remote sensing, high-resolution remote sensing, image processing, and artificial intelligence.

Dr. Zhang is a Fellow of the IEE, Executive Member (Board of Governor) of the China National Committee of International Geosphere-Biosphere Programme, Executive Member of the China Society of Image and Graphics, etc. He regularly serves as a Cochair of the series SPIE Conferences on Multispectral Image Processing and Pattern Recognition, Conference on Asia Remote Sensing, and many other conferences. He edits several conference proceedings, issues, and Geoinformatics Symposiums. He also serves as an Associate Editor of the *International Journal of Ambient Computing and Intelligence*, *International Journal of Image and Graphics*, *International Journal of Digital Multimedia Broadcasting*, *Journal of Geo-spatial Information Science*, *Journal of Remote Sensing*, and the IEEE TRANSACTIONS ON GEOSCIENCE AND REMOTE SENSING.



Bo Du (M'10) received the B.S. degree from Wuhan University, Wuhan, China, in 2005 and the Ph.D. degree in photogrammetry and remote sensing from the State Key Laboratory of Information Engineering in Surveying, Mapping and Remote Sensing, Wuhan University, in 2010.

He is currently an Associate Professor with the School of Computer, Wuhan University. His major research interests include pattern recognition, hyperspectral image processing, and signal processing.